Supporting Information

Synergistic Cobalt-Manganese Prussian Blue Analogues for Enhanced Polysulfide Conversion in Lithium-Sulfur Batteries

Kexin Yang, Yanjun Liu, Bolin Ma, Jie Wang, and Jiarui He*

Email: hejiarui123@sina.com

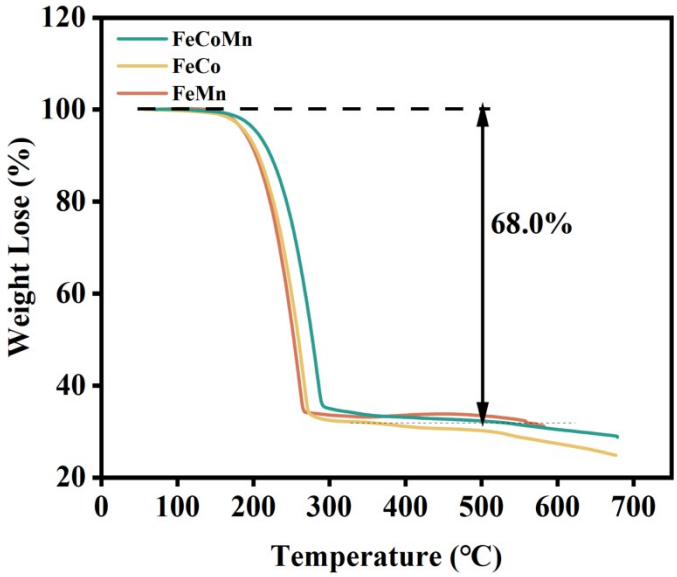

Figure.S1 Thermogravimetric analysis (TGA) curves of FeCoMn-PBA/S, FeCo-PBA/S, and FeMn-PBA/S.

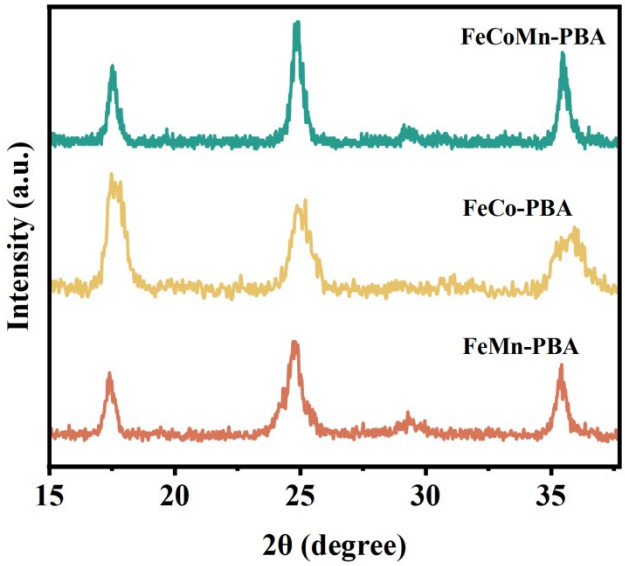

Figure S2. Refined XRD patterns of FeMn-PBA, FeCo-PBA, and FeCoMn-PBA.

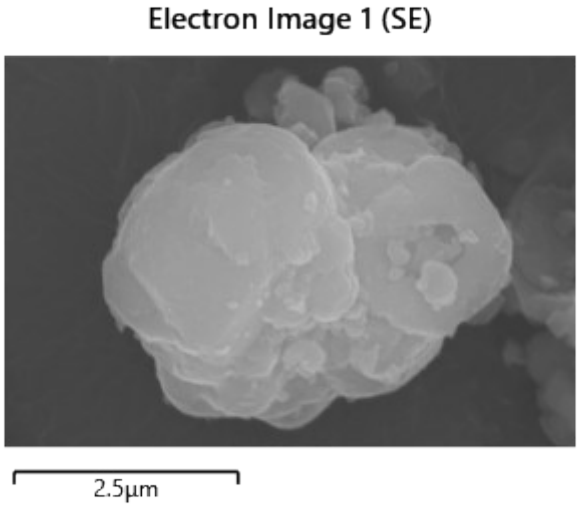

Figure S3. EDS elemental mapping overlay of FeCoMn-PBA/S.

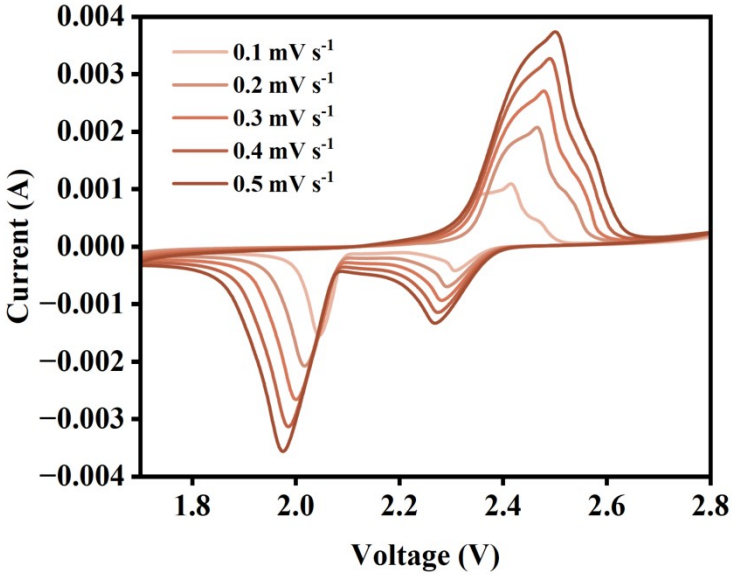

Figure S4. Consecutive CV curves of FeMn-PBA/S.

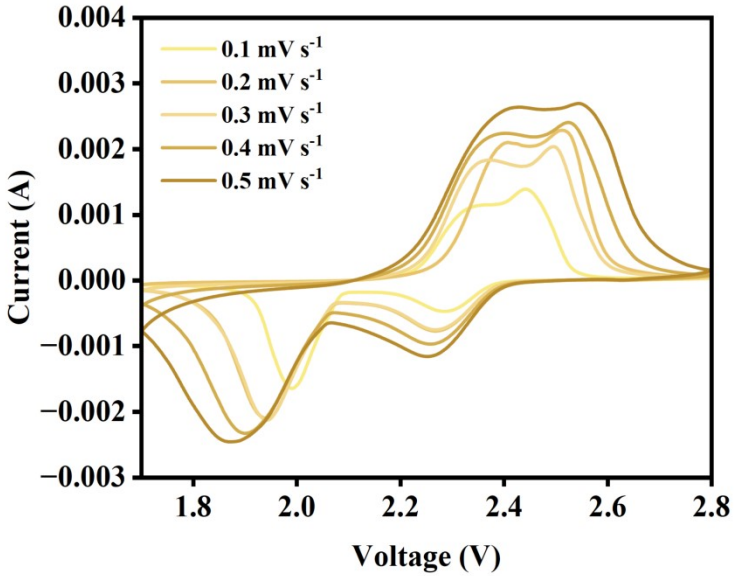

Figure S5. Consecutive CV curves of FeCo-PBA/S.

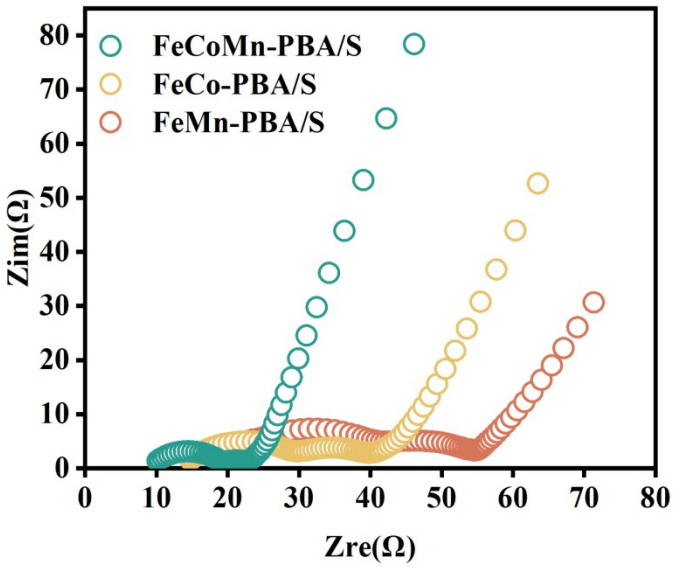

Figure S6. Electrochemical impedance spectroscopy (EIS) of FeCoMn-PBA/S, FeCo-PBA/S, and FeMn-PBA/S after charge/discharge cycling at 0.1 C.

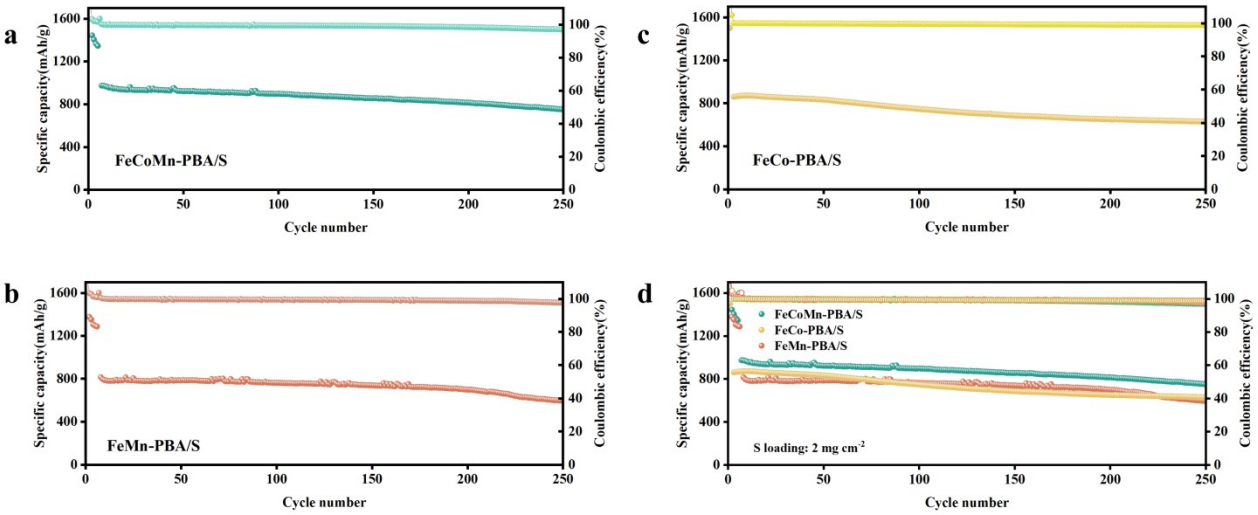

Figure S7. Long-term cycling performance of (a) FeCoMn-PBA/S, (b)FeMn-PBA/S, and (c) FeCo-PBA/S cathodes at 0.1 C.

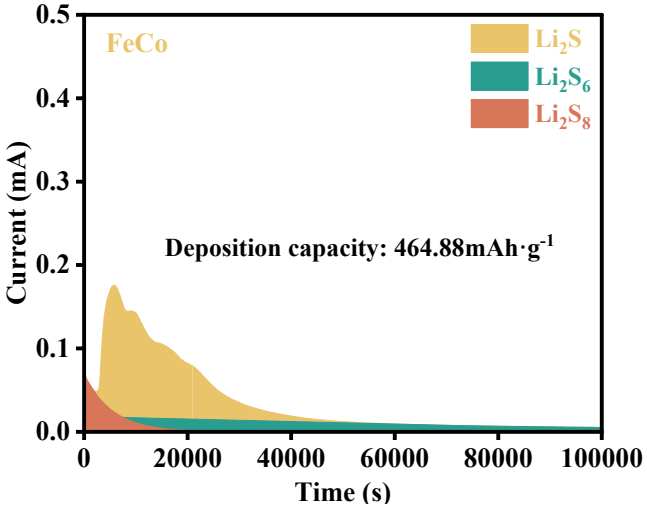

Figure S8. Potentiostatic discharge profiles for Li_2S deposition on FeCo-PBA/S.

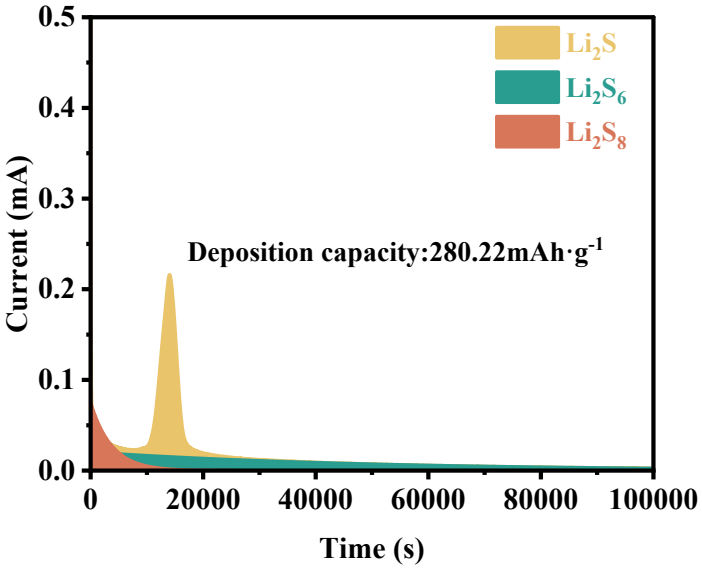

Figure S9. Potentiostatic discharge profiles for Li_2S deposition on S/C.

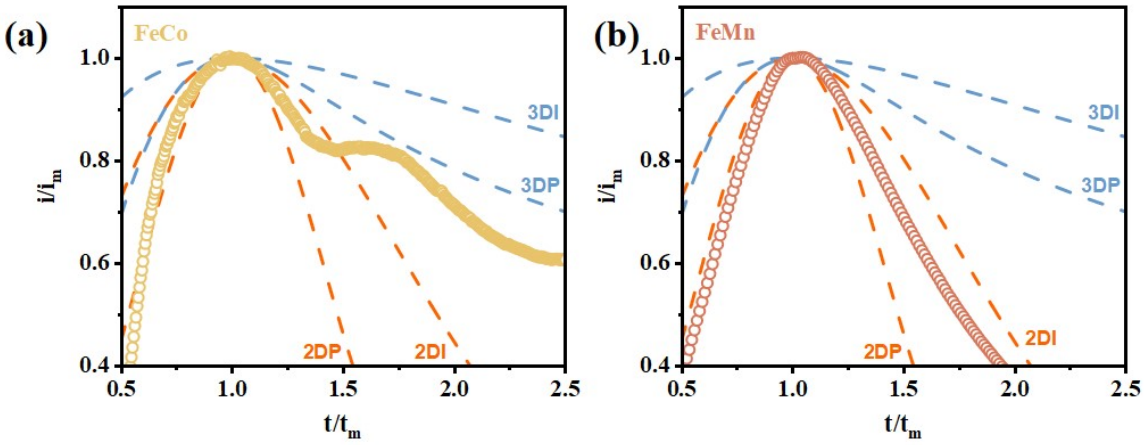

Figure S10. Dimensionless current-time transient profiles of (a) FeCo-PBA, and (b) FeMn-PBAcompared with theoretical nucleation models.

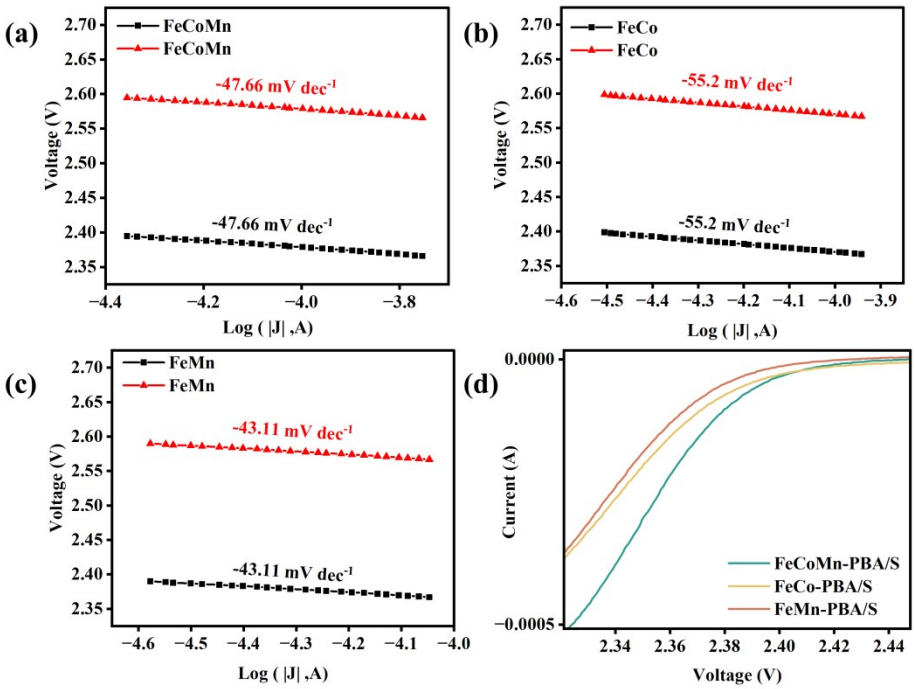

Figure S11. Electrochemical kinetic analysis of the different electrodes. Tafel plots of (a) FeCoMn-PBA/S, (b)FeCo-PBA/S, and (c) FeMn-PBA/S derived from the CV curves, respectively. (d) Zoomed-in view of the CV curves at the oxidation onset potential region to compare the reaction barriers.

Materials	S_{BET} (m^2 g^{-1})	Distribution of pore size %		
		⩽2nm	2-50nm	⩾50nm
FeCoMn-PBA/S	57.03	5.6	71.8	22.6
FeCo-PBA/S	11.63	5.7	45.9	48.4
FeMn-PBA/S	3.52	8.7	53.7	37.6

Table S1. Pore size distributions of FeMn-PBA, FeCo-PBA, and FeCoMn-PBA.

Materials	Consist	Sulfur loading (mg cm^{-2})	Initial capacity (mAh g^{-1}, 0.1 C)	Rate capacity (mAh g^{-1})	Retention ratio
FeMn-PBA/S (This working)	Fe, Mn	1.8-2.2	1286.65 (0.1 C)	0.1 C: 980.6; 0.2 C: 890.5; 0.5 C: 730.1; 1 C: 679.4; 2 C: 626.7	0.5 C/350 Cycle 59.72%
FeCo-PBA/S (This working)	Fe, Co	1.8-2.2	1185.12 (0.1 C)	0.1 C: 1043.6; 0.2 C: 961.4; 0.5 C: 866.4; 1 C: 796.7; 2 C: 725.8	0.5 C/350 Cycle 53.0%
FeCoMn-PBA/S (This working)	Fe, Co, Mn	1.8-2.2	1365.52 (0.1 C)	0.1 C: 1114.8; 0.2 C: 1051.6; 0.5 C: 966.7; 1 C: 907.4; 2 C: 836.9	1 C/500 Cycle 66.4%
FeCoNi-PBA/S/PPy (2021)	Fe, Co, Ni	1.2-1.4	1369.3 (0.1 C)	0.5 C: 490	0.1 C/100 Cycle 51.4%
FeCoNi-PBA/S (2021)	Fe, Co, Ni	—	1234.7 (0.1 C)	0.5 C: 360	0.1 C/100 Cycle 36.5%
FeCo-PBA/S (2021)	Fe, Co	—	1029.4 (0.1 C)	0.5 C: 250	0.1 C/100 Cycle 36.0%
FeNi-PBA/S (2021)	Fe, Ni	—	1303.2 (0.1 C)	0.5 C: 186	0.1 C/100 Cycle 15.9%
FeCo-PBA/S (2022)	Fe, Co	—	—	5 A g^{-1} (5 C: 811.86)	2 C/100 Cycle 789.7 mAh g^{-1}
FeMn-PBA@rGO (2024)	Fe, Mn	—	1145 (0.2 C)	—	—
Defect-rich FeCoPBA/S (2024)	Fe, Co	5.0 (High sulfur loading)	—	5 C: 583	2 C/2000 Cycle 64.3%
HE-PBA (2024, (Mn/Co/Ni/Cu/Zn)	Mn, Co, Ni, Cu, Zn	—	—	—	2 C/1000 Cycle 0.05%/Cycle

Table S2. A comparison with previously reported PBA-based sulfur hosts.

Materials	Capacity (mAh)	Weight (g)	Specific capacity (mAh g^{-1})
FeCoMn-PBA/S	0.52	0.00128	406.69
FeCo-PBA/S	0.21	0.00128	165.15
FeMn-PBA/S	0.59	0.00128	464.88
S/C	0.21	0.00128	280.22

Table S3. Calculation of Li_2S deposition capacities on different PBA electrodes.

Materials	Nucleation overpotential (mV)	Activation overpotential (mV)
FeCoMn-PBA/S	63.01	121.54
FeCo-PBA/S	66.52	111.68
FeMn-PBA/S	44.82	219.32

Table S4. Nucleation and activation overpotentials of different electrodes derived from GITT measurements.